Monitoring and analysis of pendant droplets evaporation using bare and monolayer-coated optical fiber facets

Eyal Preter,[1] Rachel A. Katims,[1,2] Vlada Artel,[1,3] Chaim N. Sukenik,[3] Denis Donlagic,[4] and Avi Zadok[1,*]

[1]*Faculty of Engineering, Bar-Ilan University, Ramat-Gan 52900, Israel*
[2]*Permanently with Binghamton University, 400 Vestal Parkway East, Binghamton, NY 13902, USA*
[3]*Departmaent of Chemistry, Faculty of Exact Sciences, Bar-Ilan University, Ramat-Gan 52900, Israel*
[4]*Faculty of Electrical Engineering and Computer Science, University of Maribor, 2000 Maribor, Slovenia*
[*]*Avinoam.Zadok@biu.ac.il*

Abstract: The monitoring of sub nano-liter pendant liquid droplets, during their evaporation from the cleaved facet of a standard optical fiber, is proposed and demonstrated. The combined reflections of incident light from the two boundaries, between fiber and liquid and between liquid and air, give rise to interference fringes as the fluid evaporates. The analysis of the fringe pattern allows for the reconstruction of the instantaneous size and evaporation rate of the droplets. These, in turn, provide information regarding the properties of the liquid itself, and the surface to which it is applied. The sensor readout is validated against direct video observation of evaporating droplets. Several examples illustrate the potential of the proposed sensor. Evaporation dynamics measurements identify the ethanol contents in binary ethanol-water mixtures with 2% certainty. The evaporation dynamics are modified by the application of a hydrophobic self-assembled monolayer coating to the tip of the fiber. Ten different organic solvents are accurately classified by clustering analysis of their evaporation data, collected using bare and coated fibers. Potential applications of the sensors could include quality control of water, beverages and oils, recognition of flexible fuel blends and fuel dilutions, mobile point-of-care diagnostics, and laboratory analysis of surface treatments.

OCIS codes: (060.2370) Fiber optics sensors; (120.2230) Fabry-Perot; (160.4890) Organic materials; (000.1570) Chemistry.

References and links

1. I. Langmuir, "The constitution and fundamental properties of solids and liquids. II. Liquids," J. Am. Chem. Soc. **39**(9), 1848–1906 (1917).
2. T. P. Bigioni, X. M. Lin, T. T. Nguyen, E. I. Corwin, T. A. Witten, and H. M. Jaeger, "Kinetically driven self assembly of highly ordered nanoparticle monolayers," Nat. Mater. **5**(4), 265–270 (2006).
3. A. P. Kryukov, V. Y. Levashov, and S. S. Sazhin, "Evaporation of diesel fuel droplets: kinetic versus hydrodynamic models," Int. J. Heat Mass Transfer **47**(12-13), 2541–2549 (2004).
4. H. Yildirim Erbil and R. Alsan Meric, "Evaporation of sessile drops on polymer surfaces: Ellipsoidal cap geometry," J. Phys. Chem. B **101**(35), 6867–6873 (1997).
5. T. A. Nguyen, A. V. Nguyen, M. A. Hampton, Z. P. Xu, L. Huang, and V. Rudolph, "Theoretical and experimental analysis of droplet evaporation on solid surfaces," Chem. Eng. Sci. **69**(1), 522–529 (2012).
6. K. Birdi, D. Vu, and A. Winter, "A study of the evaporation rates of small water drops placed on a solid surface," J. Phys. Chem. **93**(9), 3702–3703 (1989).
7. C. Liu and E. Bonaccurso, "Microcantilever sensors for monitoring the evaporation of microdrops of pure liquids and mixtures," Rev. Sci. Instrum. **81**(1), 013702 (2010).
8. P. Innocenzi, L. Malfatti, S. Costacurta, T. Kidchob, M. Piccinini, and A. Marcelli, "Evaporation of ethanol and ethanol-water mixtures studied by time-resolved infrared spectroscopy," J. Phys. Chem. A **112**(29), 6512–6516 (2008).

#203721 - $15.00 USD Received 6 Jan 2014; revised 18 Feb 2014; accepted 23 Feb 2014; published 1 Apr 2014

9. K. T. V. Grattan and B. T. Meggitt, *Optical Fiber Sensor Technology: Volume 4: Chemical and Environmental Sensing* (Kluwer, 2010).
10. N. D. McMillan, F. Fortune, O. Finlayson, D. D. G. McMillan, D. Townsend, D. Daly, and M. Dalton, "A fiber drop analyzer: A new analytical instrument for the individual, sequential, or collective measurement of the physical and chemical properties of liquids," Rev. Sci. Instrum. **63**(6), 3431–3454 (1992).
11. V. Salazar-Haro, V. Márquez-Cruz, and J. Hernández-Cordero, "Liquids analysis using back reflection single-mode fiber sensors," Proc. SPIE **8011**, 80114W, 80114W-10 (2011).
12. E. Preter, B. Preložnik, V. Artel, C. N. Sukenik, D. Donlagic, and A. Zadok, "Monitoring the evaporation of fluids from fiber-optic micro-cell cavities," Sensors (Basel) **13**(11), 15261–15273 (2013).
13. E. Preter, V. Artal, C. N. Sukenik, D. Donlagic, and A. Zadok, "Fiber optic monitoring of fluid evaporation," in *Optical Sensors (Sensors) 2013*, Technical Digest (Online) (Optical Society of America, 2013), paper SM3C.5. *http://www.opticsinfobase.org/abstract.cfm?URI=Sensors-2013-SM3C.5*
14. S. Uemura, M. Stjernström, J. Sjödahl, and J. Roeraade, "Picoliter droplet formation on thin optical fiber tips," Langmuir **22**(24), 10272–10276 (2006).
15. R. Picknett and R. Bexon, "The evaporation of sessile or pendant drops in still air," J. Colloid Interface Sci. **61**(2), 336–350 (1977).
16. D. H. Shin, S. H. Lee, J.-Y. Jung, and J. Y. Yoo, "Evaporating characteristics of sessile droplet on hydrophobic and hydrophilic surfaces," Microelectron. Eng. **86**(4-6), 1350–1353 (2009).
17. C. Liu, E. Bonaccurso, and H.-J. Butt, "Evaporation of sessile water/ethanol drops in a controlled environment," Phys. Chem. Chem. Phys. **10**(47), 7150–7157 (2008).
18. X. Shu, B. A. Gwandu, Y. Liu, L. Zhang, and I. Bennion, "Sampled fiber Bragg grating for simultaneous refractive-index and temperature measurement," Opt. Lett. **26**(11), 774–776 (2001).
19. J. A. Curcio and C. C. Petty, "The near infrared absorption spectrum of liquid water," JOSA **41**(5), 302 (1951).
20. K. Sefiane, L. Tadrist, and M. Douglas, "Experimental study of evaporating water-ethanol mixture sessile drop: influence of concentration," Int. J. Heat Mass Transfer **46**(23), 4527–4534 (2003).
21. R. J. Riobóo, M. Philipp, M. A. Ramos, and J. K. Krüger, "Concentration and temperature dependence of the refractive index of ethanol-water mixtures: Influence of intermolecular interactions," Eur Phys J E Soft Matter **30**(1), 19–26 (2009).
22. A. Ulman, "Formation and structure of self-assembled monolayers," Chem. Rev. **96**(4), 1533–1554 (1996).
23. I. Bakish, V. Artel, T. Ilovitsh, M. Shubely, Y. Ben-Ezra, A. Zadok, and C. N. Sukenik, "Self-assembled monolayer assisted bonding of Si and InP," Opt. Mater. Express **2**(8), 1141–1148 (2012).
24. M. Schuerenberg, C. Luebbert, H. Eickhoff, M. Kalkum, H. Lehrach, and E. Nordhoff, "Prestructured MALDI-MS sample supports," Anal. Chem. **72**(15), 3436–3442 (2000).
25. L. Snyder, "Classification of the solvent properties of common liquids," J. Chromatogr. A **92**(2), 223–230 (1974).
26. L. Snyder, "Classification of the solvent properties of common liquids," J. Chromatogr. Sci. **26**(11), 774–776 (1978).
27. J. MacQueen, "Some methods for classification and analysis of multivariate observations," in *Proceedings of the Fifth Berkeley Symposium on Mathematical Statistics and Probability:* Volume 1, M. L. Le Cam and J. Neyman, ed. (University of California Press, Berkeley, Calif, 1967), pp. 281–297.
28. D. Janssen, R. De Palma, S. Verlaak, P. Heremans, and W. Dehaen, "Static solvent contact angle measurements, surface free energy and wettability determination of various self-assembled monolayers on silicon dioxide," Thin Solid Films **515**(4), 1433–1438 (2006).

1. Introduction

Evaporation is a transition from the liquid phase to the gas phase that occurs at temperatures below the boiling point at a given pressure. Evaporation occurs when fluid molecules near the boundary with surrounding air are moving in the proper direction and have enough thermal energy to escape from the liquid [1]. The dynamics of the process are related to properties of the fluid itself, the ambient environment and the surface on which the fluid is applied. The study of geometry, formation and evaporation of droplets can provide information on numerous properties of liquids, such as surface tension, viscosity, chemical composition of solutions and refractive index. Monitoring the dynamics of droplet evaporation has found diverse potential applications, including monolayer deposition [2], combustion efficiency of fuels [3] and surface characterization of polymers [4]. The most widely employed method in the study of droplets evaporation is direct visual observation, using optical magnification and recording equipment [5]. Other techniques include the use of micro-gravimeters [6], micro-cantilevers [7], and time resolved infrared spectroscopy [8]. These techniques provide high accuracy, but some are inadequate for sub-nano-liter droplets volumes, and all require auxiliary equipment in the immediate surroundings of the liquid under test.

#203721 - $15.00 USD Received 6 Jan 2014; revised 18 Feb 2014; accepted 23 Feb 2014; published 1 Apr 2014

Optical fibers constitute an exceptional sensing platform. They provide remote access to potentially harsh environments, and can be readily embedded within a structure under test. Due to their small cross-section, they may serve as minimally-intrusive, bio-compatible probes [9]. The commonly observed quantities in the fiber optic monitoring of fluids are either their refractive indices or their absorption spectra. Pendent droplet analysis using optical fibers was previously reported, yet earlier works focused on the droplet formation in a capillary configuration [10] or on droplets at a steady-state [11], and did not examine the dynamics of the evaporation process. In a recent work, we proposed the use of all-fiber micro machined micro-cells for the evaporation monitoring of sub-nano-liter volume droplets, and demonstrated the recognition of few organic solvents based on their evaporation dynamics [12]. However, micro cells-based monitoring cannot directly determine the droplet size during evaporation, micro-cells fabrication requires specialty fibers, and the devices can be relatively fragile.

Herein we propose to use the cleaved facet of a standard fiber as an evaporation sensor. In this method, the reflections from a pendant fluid droplet located at the tip of the fiber are monitored. The two boundaries, between fiber and liquid and between liquid and air, give rise to interference fringes which vary as the fluid evaporates. The rate of evaporation could be determined by an analysis of these fringes [13]. The sensor is extremely simple to prepare and handle, but nevertheless provides an accurate measurement of the instantaneous evaporation rate.

In the following we first present a control experiment, in which good agreement is found between the proposed sensor configuration and direct visual observation of the evaporating droplet. Second, the sensor is employed to experimentally validate a theoretical model, proposed in [5], for evaporation dynamics of pico-liter droplets. Next, the study of evaporation of water – ethanol binary mixtures is presented. The mixing ratios of the solutions are properly identified by the proposed sensor, with 2% accuracy. Last, the evaporation of water and of ten different organic solvents are examined, before and after the deposition of a single-molecule hydrophobic coating on the fiber facet. A comparative study of the initial droplet lengths formed on bare and coated fibers, and of their evaporation times, allows for the unambiguous recognition of all ten solvents through clustering analysis. A connection was experimentally established between the lengths of droplets formed on a coated fiber and the polarity of the liquid. The results illustrate the potential of the proposed sensor as a simple and instructive tool for the analysis of both liquids and surface treatments.

2. Principle of operation and validation

A droplet of length L on the facet of a standard fiber makes for a low-finesse Fabry-Perot resonator (see Fig. 1). As the droplet evaporates its length decreases. Simple observation of interference fringes in the temporally-varying pattern of reflected optical power allows for the reconstruction of the variations in the instantaneous length of the liquid droplet. Every interference cycle, from maximum reflected power to minimum and back, corresponds to a variation in the droplet length by half the wavelength in the liquid medium.

In the experiments reported below, light from a 1 mW laser diode source at 1543 nm wavelength was launched into the first port of optical circulator. The second port of the circulator was connected to a standard single mode fiber with a cleaved facet, to which the liquid droplets were applied. The reflected light was routed through port 3 of the circulator to a low-bandwidth optical power meter. A similar apparatus with a fused silica capillary fiber was used in [14].

#203721 - $15.00 USD Received 6 Jan 2014; revised 18 Feb 2014; accepted 23 Feb 2014; published 1 Apr 2014

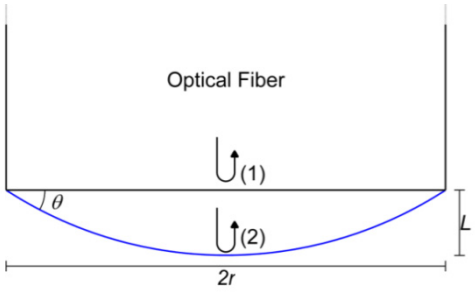

Fig. 1. Illustration of a pendant droplet of length *L* on the facet of a standard fiber of cladding radius *r*. Light is reflected at the boundaries between fiber and liquid, and between liquid and air. The contact angle of the liquid droplet is denoted by θ.

To validate the proposed method, a first set of experiments was carried out in synchronization with visual observation of the droplets, using real-time video recording at 25 frames per second. In these experiments, 20 micro-liters of doubly-distilled water were placed on a carrier silicon wafer that was pre-coated with a hydrophobic layer. The wafer was fixed to the moving stage of a contact-angle goniometer, and the fiber tip was held perpendicularly above the stage. At the beginning of each test, the fiber was immersed 1-mm into the water and the stage was then lowered. A sub-nano-liter droplet remained on the fiber facet. Reflected power from the fiber facet and images of the droplet were both recorded during evaporation. Figure 2(a) shows example frames of the droplet and its edges. The reflected optical power as a function of time is presented in Fig. 2(b). The instantaneous droplet length, as calculated using both methods, is shown in Fig. 2(c). The blue curve was reconstructed using the fringe analysis, whereas the red curve was calculated from the captured frames using image processing tools. Good agreement is found. The evaporation time was 3.5 sec. The reflected power pattern consisted of 65 fringes, suggesting that the initial droplet length was 37 μm. Due to mechanical alignment inaccuracies, the final 5 μm of the evaporation process were hidden from the camera.

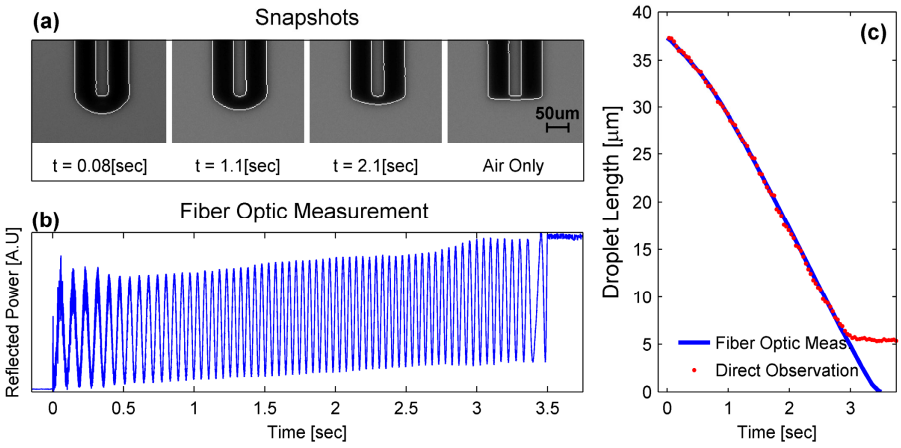

Fig. 2. (a) Image frames of the tip of a cleaved fiber with a pendent water droplet, captured during droplet evaporation within a contact angle goniometer. (b) Reflected optical power *versus* time, obtained during evaporation, showing interference fringes. Note that the detector readout is displayed on an arbitrary linear scale. The reflected power at the beginning and the end of the evaporation process is nonzero. (c) Droplet thickness as a function of time, reconstructed using image processing (red dots) and analysis of reflected power (blue curve).

The accuracy in the estimate of the droplet length using direct observation is limited by the numerical aperture of the imaging optics and the pixel size. Based on certain assumptions

#203721 - $15.00 USD Received 6 Jan 2014; revised 18 Feb 2014; accepted 23 Feb 2014; published 1 Apr 2014

regarding the droplet geometry, and using image-processing tools, the accuracy of droplet size estimate using direct observation can be improved to 0.25 μm, or below 1% in our case. Measurement uncertainties of 4.8% were reported in the literature [16]. The length estimation accuracy of the proposed sensor is limited by the proper recognition of the first and last fringes in the reflected power pattern, and is therefore on the order of 0.5 μm. Measurements of the evaporation rate using direct observation are limited to the frame rate of the recording camera, which is typically 25 frames per second. The bandwidth of the photo-detector and the sampling rate of the processing electronics can be orders of magnitude larger. The fiber-based sensor is therefore scalable to the monitoring of much faster evaporation rates.

The pendent droplet can be modeled as a spherical cap [15], and represented by two parameters: the droplet length L and the contact radius r. The contact angle is defined as the angle formed where the liquid boundary meets the solid surface: $\tan(\theta/2) = L/r$ (see Fig. 1). Two regimes of sessile droplet evaporation are reported in the literature: (a) Evaporation with a constant contact angle, where both the length and the base area of the droplet decrease with time while the contact angle remains fixed; and (b) Evaporation with a constant contact radius, in which the rim of the droplet is pinned and the contact angle reduces with time [15]. The evaporation of water droplets from hydrophilic surfaces is typically characterized by small contact angles and a constant radius [16]. In our experiments, we observed a comparatively small contact angle of 61.5° and a constant radius which equals that of the fiber (Fig. 2(a)), in agreement with expectations.

3. Experiments and results

3.1 Evaporation dynamics of sub nano-litter water droplet

Several experiments had shown that in the evaporation of comparatively large (r~1mm) water droplets, the squared third root of droplet volume ($V^{2/3}$) decreases linearly with time [17]. In contrast, a recent theoretical prediction suggested that the volume V of a small evaporating droplet is expected to vary linearly with time [5], rather than $V^{2/3}$. However, a corresponding experiment was not yet reported. Using our sensor, we are able to provide experimental evidence in support of the proposed model. In this set of experiments we studied the relation between droplet volume and time during the evaporation of small water droplets, with a constant radius which equals that of the fiber. Figure 3 shows the reconstructed droplet volume V (a) and $V^{2/3}$ (b) as a function of time. It was found that V follows a linear dependence more closely (R^2 = 0.999) than $V^{2/3}$ (R^2 = 0.99), corroborating the theoretical prediction.

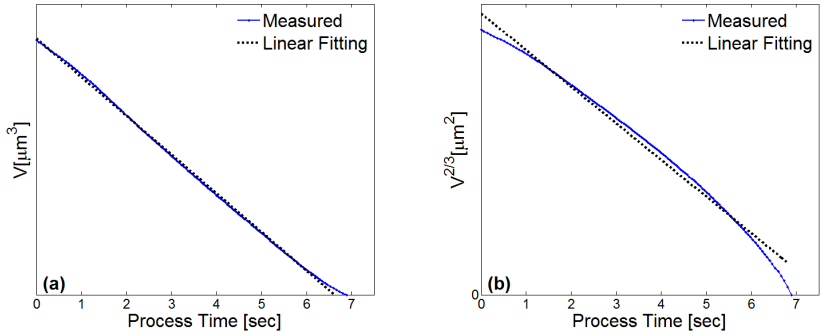

Fig. 3. Reconstructed dimensions of doubly-distilled, evaporating water droplets as a function of time. (a) Droplet volume V; (b) Third root of the volume squared $V^{2/3}$.

#203721 - $15.00 USD Received 6 Jan 2014; revised 18 Feb 2014; accepted 23 Feb 2014; published 1 Apr 2014

3.2. Temperature effects

Figure 4(a) shows the accumulated change in the length of water droplets, during their evaporation at different ambient temperatures, as collected by the fiber tip sensor. The droplets were drawn from a water reservoir that was held at a constant temperature of 19 °C throughout the entire set of experiments, whereas the ambient temperature was raised from 19 °C to 24 °C and 28 °C. The evaporation rate becomes faster with temperature, as expected. In addition, the standard deviation between the evaporation rates of repeating experiments increases with temperature as well: from ± 0.07 μm/sec at 19 °C to ± 0.16 μm/sec at 28 °C. The thermal variations in the refractive index of water within this temperature range are negligible [18].

The intensity of the interrogating light could also affect the evaporation dynamics. The absorption coefficient of light at 1550 nm wavelength in water at 20 °C is 15 cm^{-1} [19]. Hence about 6% of the energy of the incident light is converted to heat within the droplet length. Figure 4(b) shows the rates of evaporation of water droplets at a temperature of 19 °C, as estimated by the fiber-tip sensor with different interrogating intensities. The evaporation rate of 5.5 μm/sec is independent of the interrogating optical power below 1 mW, and it increases with higher power levels. The effect of a power increase from 1 mW to 3 mW on the rate of evaporation is comparable to that of a 15 °C increase in the ambient temperature.

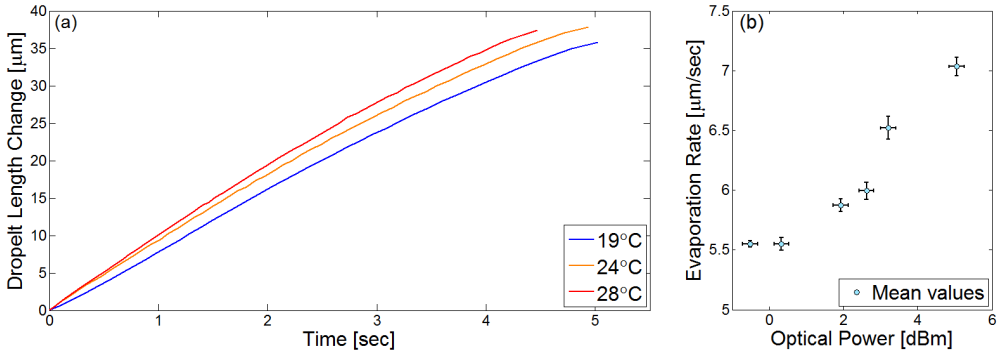

Fig. 4. (a) Accumulated change in the lengths of water droplets as a function of time, recorded during evaporation from a fiber tip sensor at different ambient temperatures. (b) Rates of evaporation of water droplets from a fiber tip sensor at a fixed temperature, estimated using different power levels of the interrogating light.

3.3 Evaporation of ethanol-water binary mixtures

The evaporation of droplets of ethanol-water mixtures was the subject of extensive studies over the last decade. The evaporation dynamics of these mixtures can be divided to three phases. In the first phase, evaporation takes place at an almost constant rate, which increases with the relative concentration of ethanol in the mixture. Following a transitional, second phase, the third and final phase of evaporation is once again of a constant rate, which corresponds to that of pure water [8,17,20]. Liu and coauthors [17] suggested that the following three processes govern the evaporation of water-ethanol mixture droplets: 1) ethanol flow to the surface of the droplet due to diffusion; 2) the fundamental evaporation of ethanol; and 3) the fundamental evaporation of water.

Herein the evaporation properties of water-ethanol mixtures are explored using the fiber tip sensor. Five different mixtures of ethanol and doubly-distilled water were prepared and tested, as well as pure water and almost pure (>99.5%) ethanol. The concentrations of ethanol and water in all mixtures are defined according to their relative volumes. Each test was carried out between 4 and 6 times, using the setup and procedure described in section 2. For a simpler comparison, the analysis is presented in terms of the accumulative change in droplet

#203721 - $15.00 USD Received 6 Jan 2014; revised 18 Feb 2014; accepted 23 Feb 2014; published 1 Apr 2014

length since the onset of evaporation. Figure 5 shows that each mixture has a different temporal profile of evaporation. As expected, the evaporation rate increases with the ratio of ethanol in the mixture. Environmental fluctuations, liquid impurities and measurement noises cause small variations among repeating experiments of nominally identical samples.

The expected, three-phase evaporation dynamics are observed in the experiments. For example, Fig. 6(a) illustrates the droplet length during the evaporation of 1:1 water-ethanol mixture. The initial and final phases of the process are of almost constant rates, and the initial rate of evaporation is considerably higher than that of subsequent dynamics. The evaporation rate at the initial phase decreases with the relative concentration of water in the mixture (Fig. 6(b)), until it approaches that of pure water (about 62 $\mu m \cdot sec^{-1}$).

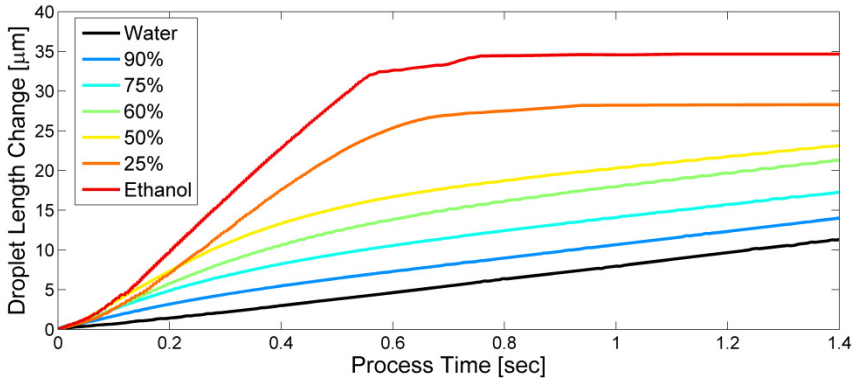

Fig. 5. Accumulated change in droplet lengths during evaporation of water-ethanol mixtures, measured using the fiber-tip sensor. Black: pure distilled water. Red: pure ethanol. Mid-tones: see legend

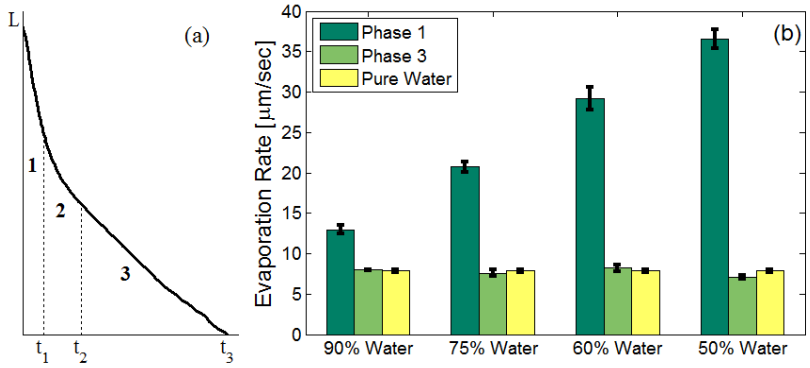

Fig. 6. (a) Illustration of the instantaneous length of a 1:1 water-ethanol mixture droplet, with the three-phase notation. (b) Evaporation rates of different mixtures, measured during phase 1 and phase 3, and the evaporation rate of pure water, compared with [20].

Figure 7 shows the evaporation rates in the first phase of the process, as a function of the relative concentration of water in the binary mixture. A good linear fit is achieved (R^2 = 0.998). The evaporation rate at the first phase provides a good estimate of the relative ethanol concentration, with an accuracy of about 2% (1% for water-rich mixtures). Note that a corresponding estimate based on refractive index measurements cannot be obtained, since the dependence of the refractive index on the mixing ratio is nonlinear and even not monotonous. For instance, the refractive indices at 589 nm of mixtures with 25% and 12% relative water concentrations are the same [21].

#203721 - $15.00 USD Received 6 Jan 2014; revised 18 Feb 2014; accepted 23 Feb 2014; published 1 Apr 2014

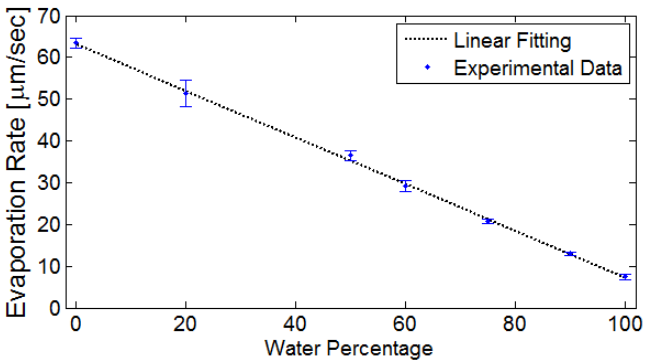

Fig. 7. Rates of evaporation in the first phase as function of the relative water concentration in water-ethanol mixtures. Black: linear fit. Blue: experimental data.

3.4 Evaporation of water droplets from a monolayer-coated fiber facet

Self-assembled monolayers (SAMs) are highly ordered two-dimensional structures that are strongly anchored to a surface [22]. Their deposition occurs spontaneously from a solution which contains the monolayer-forming molecules. These films define the surface properties, despite their nanometric thickness. The functional group at one end of the molecule attaches to a substrate, whereas the other terminus of the molecule remains free-standing and controls the chemistry of the surface. SAM coatings can be synthesized to attract or repel particular liquids, and can therefore be considered for the functionalization of optical fibers in sensing applications. In a complementary perspective, fiber optic sensing can provide a tool for the characterization of the monolayer surface treatment, as a simple alternative to the goniometry that is commonly used for such purposes. In this part, the evaporation of water droplets is examined before and after the deposition of a SAM on the fiber facet.

We deposited a SAM of octadecyltrichlorosilane (OTS, Fig. 8(a)) on the cleaved facet of a standard fiber. The deposition process was described in detail in [23]. Figures 8(b) and 8(c) show goniometer images of reference and coated fibers, immersed in water. Following OTS deposition, the hydrophilic silica surface becomes hydrophobic. When the goniometer stage was lowered, as in the experiments described in section 2 (Fig. 2), the droplet did not settle consistently at the center of the fiber, and nearly no fluid remained on the fiber tip at all (Fig. 8(d)). The off-center position of the droplet fraction on the optical fiber tip can be explained by micro-roughness that acts as an anchoring point [24]. The surface modification is clearly evident in the temporal reflectivity pattern recorded by the fiber sensor as well, as shown in Fig. 8(e). The duration of evaporation from the coated fiber is only 1 sec as opposed to 3.5 sec in Fig. 1, and no interference fringes are observed. Less complete or less organized SAM coatings would yield much less dramatic changes in the evaporation profile [13].

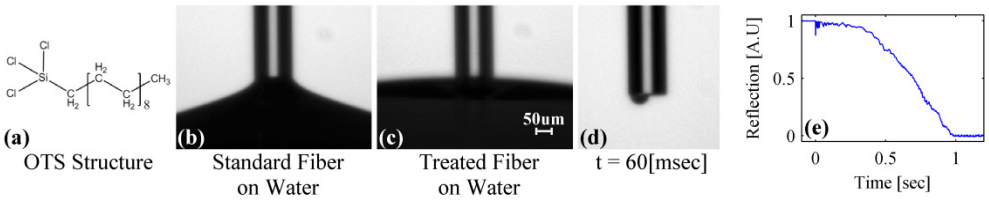

Fig. 8. (a) An OTS molecule. (b) Goniometer image of a reference fiber tip immersed in water. (c) Corresponding image of an OTS-coated fiber. (d) Only a fraction of a droplet remains on the tip of the coated fiber when removed from the water. (e) Reflected optical power as a function of time, collected during evaporation of water from the OTS-coated fiber tip. The evaporation time is short and no interference fringes are observed.

#203721 - $15.00 USD Received 6 Jan 2014; revised 18 Feb 2014; accepted 23 Feb 2014; published 1 Apr 2014

3.5 Evaporation of organic solvents from bare and monolayer-coated fibers

The evaporation of ten different organic solvents from bare and OTS SAM-coated fiber facets was monitored, using the procedures described above. Figure 9(a) shows the reflected fringe patterns collected during the evaporation of a droplet of acetone from a bare fiber tip (blue) and an OTS-coated fiber tip (red). In this example, the initial droplet size was reduced by as much as 50% following OTS monolayer treatment of the fiber facet, leading to a reduction of the total evaporation time from 0.75 sec to 0.27 sec. Nevertheless, the fringe pattern obtained from the coated fiber facet resembles the fringe pattern obtained from the bare fiber for the initial 160 ms of the evaporation, as can be seen in Fig. 9(a) and 9(b). This observation suggests that the evaporation mechanism in the beginning of the process remains unchanged, and differences are either in the initial droplet size and/or in the latter stages of evaporation.

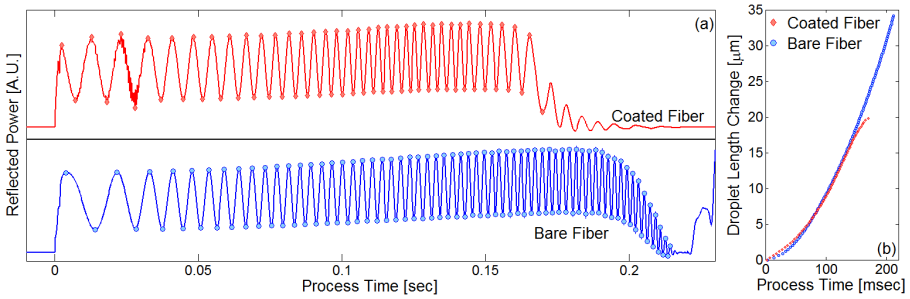

Fig. 9. (a) Reflected optical power collected during acetone evaporation from a bare fiber (blue) and an OTS coated fiber (red). The markers specify the extremum points for the fringe counting. (b) The accumulative droplet length changes as a function of time, calculated from the fringe patterns of panel (a).

Figure 10 shows the droplet length change as a function of time, reconstructed based on the fringe patterns in the evaporation profiles of ten organic solvents. In all tested liquids, the lengths of droplets formed on the bare fiber tip were 35 ± 5 μm. The corresponding lengths of droplets formed on the OTS-coated fiber were smaller, with the exception of hexane for which the two lengths were almost the same (Fig. 10, panel 9). The largest difference in droplet length of 25 μm was observed in the evaporation of acetonitrile (Fig. 10, panel 6).

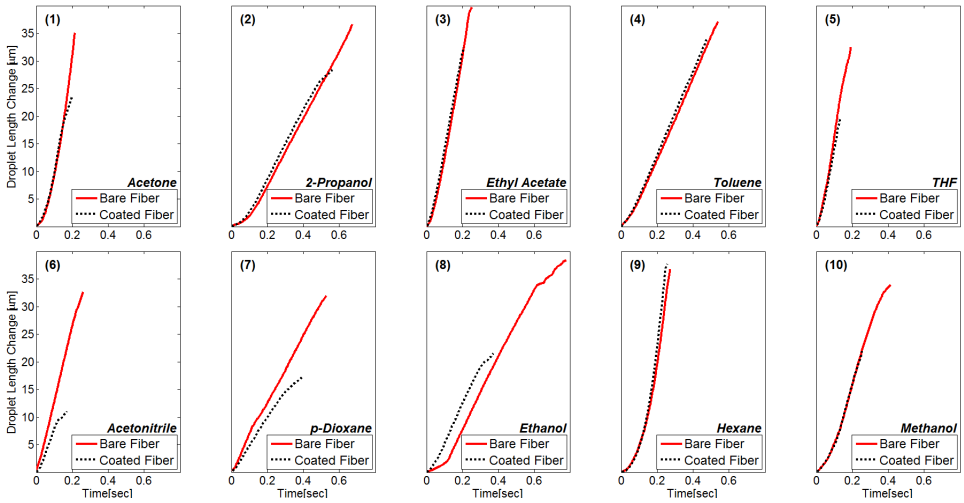

Fig. 10. Droplet length change as a function of time for ten different organic solvents, reconstructed based on evaporation from a bare fiber tip (red) and an OTS-coated tip (black).

#203721 - $15.00 USD Received 6 Jan 2014; revised 18 Feb 2014; accepted 23 Feb 2014; published 1 Apr 2014

For most of the tested solvents, the deposition of the OTS monolayer coating had little effect on the instantaneous evaporation rate, but rather on the initial droplet length (see Fig. 11(a)). While the change in acetonitrile droplet length was about 25 μm, in hexane there was no change. One property that distinguishes acetonitrile from hexane is their polarity. Snyder [25, 26] defined a descriptive polarity index based on the solvent's ability to dissolve many compounds. Polarity may also refer to surfaces. In this context, a polar surface is one that is terminated by polar molecules. Optical fibers are made of fused silica, which is naturally terminated by polar OH groups in ambient conditions. Hence the surface of a bare fiber can be considered as polar. In contrast, the surface of the OTS-coated fiber is non-polar.

In our experiments, droplets are formed on the tip of fibers as they are pulled out of a liquid reservoir. The sizes of droplets represent a balance between the strength of attachment between liquid and surface, which is pulling a mass of liquid out of the reservoir, and the inter-molecular forces of the liquid which work against it. While the former may be modified by changes in the surface polarity, the latter are not. Hence we make the following conjecture: polar liquids would form larger droplets on the surface of the bare fiber than on the surface of the OTS-coated fiber. Differences in size would be smaller for non-polar liquids.

Figure 11(b) presents the droplet length differences as a function of the fluid polarity index. The polarity values are given in [25, 26]. As predicted, solvents with a low polarity index such as hexane and toluene display comparatively smaller variations in the droplet length between the two sets of experiments, while solvents with a high polarity index are characterized by larger differences in droplets sizes. A second-order polynomial relation between the polarity index and the droplet size difference is suggested experimentally, although the fitting is not optimal. Note that the analysis is rather basic. Factors such as the surface free energy, and the potential formation of hydrogen bonds, were not taken into account. A more elaborate study, relating to the physical and chemical properties of the different liquids, would be necessary to fully account for the observations. Nevertheless, the monotonous dependence of the droplet length difference on polarity index is consistent throughout the set of experiments.

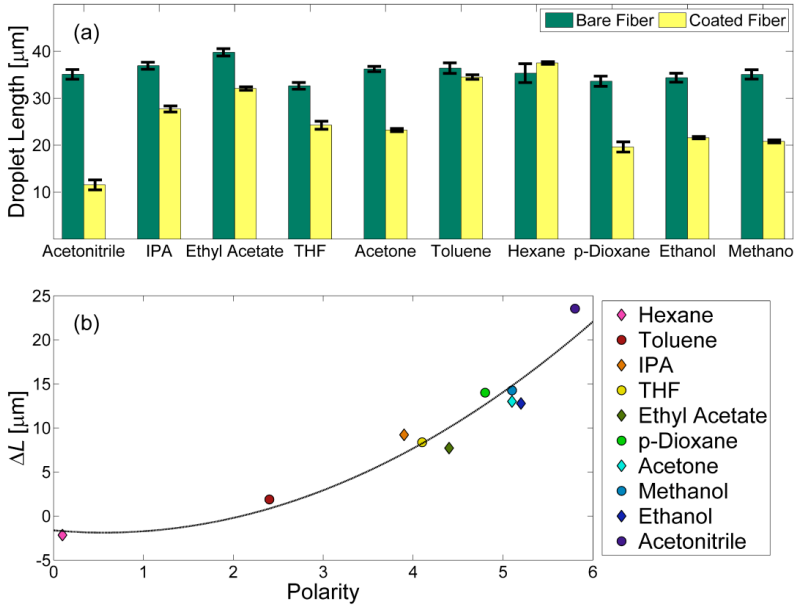

Fig. 11. (a) The droplet sizes of different organic solvents, reconstructed by firnge analysis during evaporation from a bare fiber tip (green), and from a coated fiber tip (yellow). (b) The difference in droplet lengths between the two experiments as a function of the polarity index of the solvent, with a parabolic fitting.

#203721 - $15.00 USD Received 6 Jan 2014; revised 18 Feb 2014; accepted 23 Feb 2014; published 1 Apr 2014

Lastly, we demonstrate the ability to identify a given fluid based on its evaporation properties. The experimental data presented in Fig. 10 were used in cluster analysis recognition: a method of assigning a set of objects into groups, so that the objects in the same cluster are similar to one another more than to those in other clusters. We used the *k*-means method: a technique of partitioning an *N*-dimensional population into *k* sets, on the basis of training data, with reduced in-class variance. The process is described in details at [27]. In our study, the initial samples space is the set of fringe patterns collected from the solvents mention above. The data was reduced to two parameters which represent each individual experiment: the evaporation time and the number of observed fringes. Note that the number of fringes cannot be simply related to a droplet length since the refractive index of the sample is not known in advance. The grouping of the points was done by Matlab *k*-means function using the Euclidean norm. The centroid for each cluster is the mean of the points included in it, in the two-dimensional space of the above parameters.

The analysis of evaporation data from a bare fiber tip did not converge, since the in-class variance was larger than the differences between groups (Fig. 12(a)). The numbers of fringes observed for the different solvents during evaporation from the bare fiber tip are rather similar (see also Fig. 11(a)), hence the potential fluid recognition based on the chosen parameters was limited. In contrast, good margins are achieved in the analysis of evaporation data from the OTS-coated fiber. The ten cluster centroids and the training data points are presented in Fig. 12(b). Toluene and acetonitrile have the widest margins, while smaller separation was observed for acetone, THF and methanol.

Even better results are achieved in combining bare fiber and coated fiber measurements. In Fig. 13, a three dimensional clustering based on the *k*-means method is presented. The first two dimensions are the evaporation time and the number of fringes measured with the OTS-coated fiber, and the third one is the evaporation time measured from the bare fiber tip. In this analysis the separation among THF, acetone and methanol is better than in the two-dimensional case (Fig. 12(a) and 12(b)).

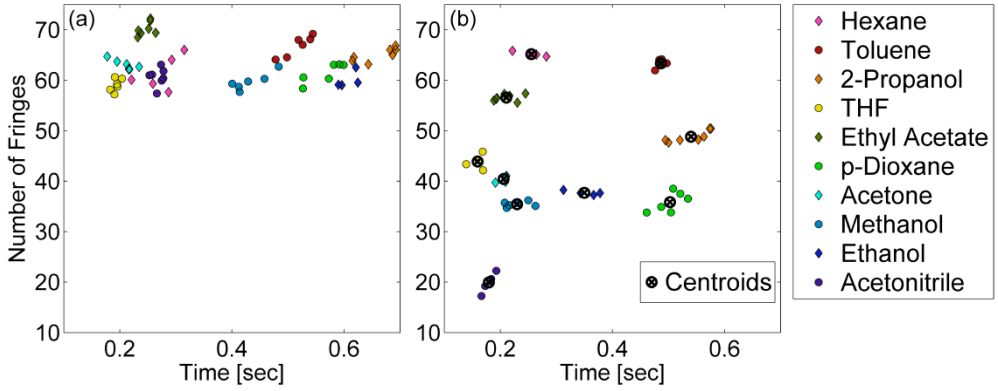

Fig. 12. Recognition of ten organic solvents based on a clustering analysis of their evaporation data. (a) using a bare fiber. Individual clusters are difficult to distinguish. (b) using an OTS-coated fiber tip. Clusters are clearly recognized.

It should be noted that the clustering analysis above is very basic. The raw data contains many more features and details than simply the number of fringes and the process time. More sophisticated analysis can be multi-dimensional, and employ additional parameters such as fringe contrast and fringe pattern envelope. Further enhancement of the data analysis could be achieved by using additional coating types. Many different SAMs can be deposited on silica surfaces [28].

#203721 - $15.00 USD Received 6 Jan 2014; revised 18 Feb 2014; accepted 23 Feb 2014; published 1 Apr 2014

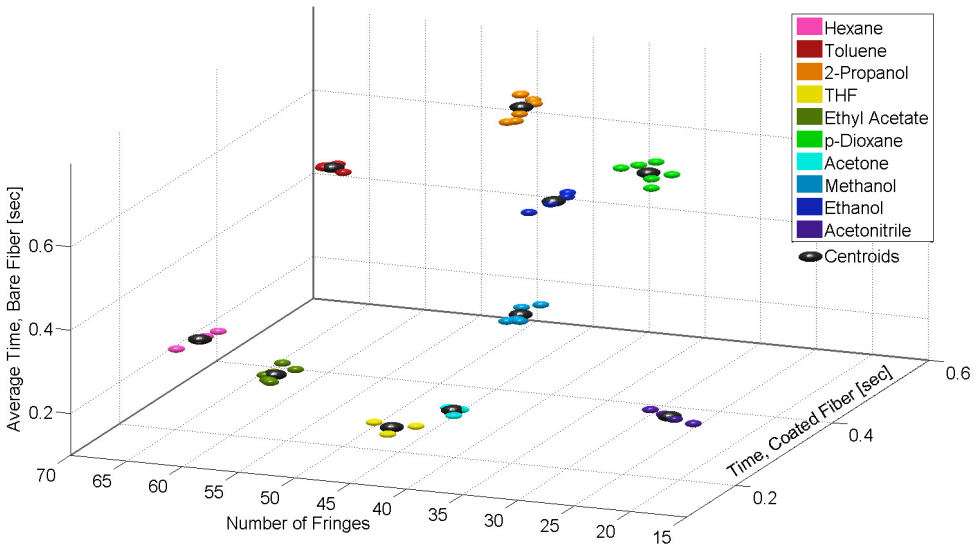

Fig. 13. Recognition of ten organic solvents based on a combined clustering analysis of their evaporation data, using an OTS-coated fiber tip and a bare fiber tip

4. Summary

We proposed and demonstrated a method for monitoring the evaporation dynamics of pendent droplets from the tip of a standard optical fiber. The method is extremely simple and economical, but nevertheless provides an accurate measure of the instantaneous droplet size and rate of evaporation. The sensor readout was validated against direct video recording of evaporating droplets. The evaporation dynamics of sub-nano-liter droplets were examined, and provided evidence in support of a theoretical analysis which was not previously corroborated. The evaporation of ethanol-water binary mixtures was shown to consist of three different phases, in agreement with the known literature. However, the fiber sensor experiment required only a few seconds, whereas corresponding measurements in a goniometer may take minutes or tens of minutes. The analysis of the evaporation rate during the first phase allowed for an estimate of the relative concentration of ethanol in the mixtures, with 2% accuracy. Unlike most known fiber-optic sensors of liquids, the method does not rely on the refractive index or the absorption spectrum of the substance being tested.

Monolayer coatings can add another dimension to the operation of the sensor, as they modify the interaction between the surface and the liquid. The formation of water droplets on the tip of an OTS-coated fiber was largely inhibited, in agreement with expectation. This change was strongly evident in the readout of the sensor. A connection was experimentally established between the size of droplets formed on the coated fiber and the polarity index of the tested liquid. Lastly, the combined analysis of the sensor readouts, collected during droplet evaporation from bare and coated fibers, allowed for the successful recognition of ten different organic solvents through clustering analysis. The ability to modify the surface properties of the fiber via monolayer deposition provides a useful extra handle for the recognition of specific fluids: coatings can be formed that specifically attach to, or repel, a particular fluid of interest. For a few of the solvents, changes in the fringe contrast were observed towards the final stages of the evaporation. Possible explanations include modifications to the droplet geometry, or an offset of remaining liquid from the center of the fiber, towards the end of the process (see also Fig. 8(d)). Quantitative analysis of the fringe contrast is outside the scope of the current work.

#203721 - $15.00 USD Received 6 Jan 2014; revised 18 Feb 2014; accepted 23 Feb 2014; published 1 Apr 2014

The proposed sensor provides a new approach the monitoring and analysis of liquids using optical fibers. Potential applications of the sensors could include quality control of water, beverages and oils, recognition of fuel dilutions, mobile point-of-care diagnostics, laboratory analysis of surface treatments etc.

Acknowledgments

This work was carried out in part within the framework of the European Union Collaboration on Science and Technology (COST) Action TD1001 OFSESA. R. A. Katims acknowledges a Summer Internship form Career Israel organization, for partial support of her stay at Bar-Ilan University.

#203721 - $15.00 USD Received 6 Jan 2014; revised 18 Feb 2014; accepted 23 Feb 2014; published 1 Apr 2014